Dalton Transactions

ROYAL SOCIETY OF CHEMISTRY

PAPER

View Article Online
View Journal | View Issue

Cite this: *Dalton Trans.*, 2024, **53**, 14364

Unravelling the mechanism of apoptosis induced by copper(II) complexes of NN_2-pincer ligands in lung cancer cells†

Athulya Das and Muniyandi Sankaralingam *

The invention of efficient chemotherapeutic drugs is essential for human health and development. Keeping this in mind, a series of copper(II) pincer complexes, **1–4**, of ligands **L1**(H) = 2-morpholino-*N*-(quinolin-8-yl)acetamide, **L2**(H) = 2-di-*n*-propylamino-*N*-(quinolin-8-yl)acetamide, **L3**(H) = 2-di-*n*-butylamino-*N*-(quinolin-8-yl)acetamide and **L4**(H) = 2-di-*n*-benzylamino-*N*-(quinolin-8-yl)acetamide have been synthesized, characterized, and utilized for inhibiting cancer proliferation. Complexes **1–4** showed very efficient activity against lung (A549) and breast (MCF-7) cancer cells, which are the most frequently diagnosed cancers according to the WHO. Among them, **1** was highly active against lung cancer cells with an IC_{50} value of 8 μM, showing no toxicity towards common L929 fibroblast cell lines (IC_{50} > 1000 μM). Moreover, AO–EB staining inferred that this cellular demise was attributed to apoptosis, which was determined to be 25.91% of cells by flow cytometry at the IC_{50} concentration. Furthermore, carboxy-H_2DCFDA staining revealed the involvement of ROS in the mechanism. Interestingly, JC-1 dye staining revealed a change in the potential of the mitochondrial membrane, which indicates the enhanced production of ROS in mitochondria. A deep search for the mechanism through *in silico* studies guided us to the fact that complexes **1–4** might perturb the function of complex I in mitochondria. Furthermore, the studies can be expanded towards clinical applications mainly with morpholine appended complex **1**.

Received 12th April 2024,
Accepted 19th July 2024

DOI: 10.1039/d4dt01075b

rsc.li/dalton

1. Introduction

According to the World Health Organization (WHO), cancer caused one among six deaths in 2018.[1] Even though the survival rate is improving, there is a long way to go for a complete cure of the disease. Lung cancer and breast cancer have become very common but an ideal treatment method is yet to be established. Therefore, scientists are on a huge thrust to develop novel, efficient drugs against this malady. As a result, recent years have witnessed the rapid expansion of metallodrugs with a wide variety of metals including transition metals.[2–7] The choice of a metal centre plays an important role because it can change the physicochemical properties of the complexes.[8,9] Moreover, biomimetic first-row transition metal complexes are found to be very promising candidates as anticancer drugs.[10] Among them, copper complexes always have a special place due to their high anticancer activity.[11–14] One of the relevant components of metallodrugs is the heterocyclic ligands that are extremely biocompatible due to the structurally relevant natural molecules.[15–17] For instance, aminoquinoline is one of the pharmacophores in medicinal chemistry involved in many applications including anticancer activities.[18–20] Similarly, along with aminoquinoline, if bioactive molecules like morpholine are used, then the activity could be enhanced.[21] Moreover, the solubility and lipophilicity can be tuned by propyl, butyl, and benzyl groups on the ligands.[22]

In the past few years, several pincer complexes of different metals have been reported to have excellent anticancer activities that can be attributed to their unique structural orientation.[23] For example, two of the aminoquinoline-based copper(II) pincer complexes were reported to have cytotoxic activity against A549 cells. Among them, one of the complexes had an IC_{50} value of 1 μM and the other was active only at a concentration as high as 1 mM.[24] In another report, two more aminoquinoline based copper(II) pincer complexes were

Bioinspired & Biomimetic Inorganic Chemistry Laboratory, Department of Chemistry, National Institute of Technology Calicut, Kozhikode-673601, Kerala, India.
E-mail: msankaralingam@nitc.ac.in, sankarjan06@gmail.com

†Electronic supplementary information (ESI) available: Detailed procedure for synthesis and lipophilicity determination. Table S1 and Fig. S1–S16 include IR spectra of **L1**(H)–**L4**(H) and **1–4**, the mass spectrum of **4**, phase images, and percentage viability diagrams of A549 and MCF-7 treated with complexes and ligand **L1**(H), phase images and percentage viability diagrams of L929 treated with **1**, UV-visible spectra of **L4**(H) and **4** for lipophilicity calculation, UV-visible spectra for complex **4** formation constant calculation, and molecular docking interactions of **2–4** with 5XTD. CCDC 2311348. For ESI and crystallographic data in CIF or other electronic format see DOI: https://doi.org/10.1039/d4dt01075b

reported with IC_{50} values of around 0.46 and 0.43–0.90 μM, respectively, against MCF-7 and A549 cell lines.[25] Another report described a series of terpyridine based copper(II) pincer complexes with good activity against A549 (IC_{50} = 4.2–100 μM) and MCF-7 (IC_{50} = 43–100 μM) cell lines.[26] Similarly, cyclometalated copper(I) pincer complexes with phosphaadamantane derivatives were reported with very good anticancer activity against A549 and MCF-7 cells, for which the IC_{50} value ranges from 2.35 to 3.92 μM and 3.08 to 8.41 μM, respectively.[27] Very recently, SNS donor copper(II) pincer complexes have been reported against A549 cells.[28] Among them, the chloro and thiocyanate derivatives were more active with IC_{50} values of around 12.30 μM. However, the perchlorate derivative had an IC_{50} value of 14.08 μM. Thus, activity mainly changes depending on the ligand donors.

As previously mentioned, morpholine (**1**), dipropyl (**2**), dibutyl (**3**), and dibenzyl (**4**) derivatives of 8-aminoquinoline based copper(II) pincer complexes (Scheme 1) were synthesized, characterized, and tested for their anticancer efficacy against MCF-7 and A549 cell lines. It should be noted that complexes **1–3** have already been proved as better antimicrobial agents from our recent study.[7] Here, with IC_{50} values ranging from 8 to 20 μM and 15 to 19.35 μM, all four complexes showed potential cytotoxicity against A549 and MCF-7 cells, respectively. The highly active complex **1** against A549 cells was found to display no toxicity towards the normal L929 fibroblast cell line (IC_{50} > 1000 μM). The dominant activity of **1** compared to its corresponding ligand **L1**(H) (IC_{50} = 77.65 μM) against A549 cells revealed the importance of the copper complexes. A detailed mechanistic investigations reveal that cell death through apoptosis, which was induced by the present copper complexes, produces excess ROS in mitochondria. Furthermore, we expect that clinical applications with morpholine appended complex **1** may be extended.[29]

2. Experimental

2.1. Materials

Chemicals purchased commercially were used without additional purification. Bromoacetyl bromide and 8-aminoquinoline were obtained from TCI Chemicals. Copper(II) bromide, triethylamine, morpholine, and diethyl ether were procured from Merck, India. Alfa Aesar supplied di-*n*-propylamine and di-*n*-butylamine. Dibenzylamine and DMSO (extra pure 99%) were procured from SRL, India. Acetone, methanol, dichloromethane, and ethyl acetate were procured from Qualigens, India. Using magnesium turnings and iodine, methanol was distilled. Calcium chloride and calcium hydride were used to distill acetone and DCM respectively. The cell lines A549 and MCF-7 were obtained from the National Centre for Cell Science (NCCS), Pune, India.

2.2. Physical measurements

Agilent Cary 8454 UV-visible and Jasco 4700 ATR-FTIR spectrometers were utilized for recording the absorption spectra and infrared spectra of the compounds, respectively. NMR spectra were recorded using a Jeol 500 MHz NMR spectrometer. Mass data were measured using an Agilent 6545 Q-TOF LC/MS instrument and a Bruker Daltonics Esquire 6000. A PerkinElmer 2400 Series II analyser was used for CHN analysis. A Bruker BioSpin spectrometer, Germany (EMXmicro A200-9.5/12/S/W), was used to collect electron paramagnetic resonance (EPR) spectra at 100 K. Calibration of the *g* value was done using a manganese marker. Magnetic measurements *viz*. zero-field cooling (ZFC) and field cooling (FC) were performed using Bruker WIN EPR acquisition and processing software in the range of 100–300 K. A Bruker D8 Venture dual source diffractometer was employed to obtain single-crystal X-ray diffraction data using Mo-Kα radiation. An Olympus fluorescence microscope, CKX-53, Japan, was used to see the cells after anticancer mechanistic studies. All the incubations for anticancer studies were under a 5% CO_2 atmosphere at 37 °C.

2.3. Synthesis of ligands and complexes

The ligands **L1**(H), **L2**(H), and **L3**(H) and their copper(II) complexes **1**, **2**, and **3** were synthesized by following our very recent reports.[6,7] The detailed synthetic steps are elaborated in the ESI.†

2.3.1. 2-Morpholino-*N*-(quinolin-8-yl)acetamide, L1(H). Beige colour powder; yield, 79(3)%. ^{1}H NMR (500 MHz, $CDCl_3$, 298 K); δ (ppm): 11.38 (s, 1H), 8.78–8.77 (dd, J = 4.58, 1.53 Hz, 1H), 8.69–8.67 (dd, J = 7.25, 1.53 Hz, 1H), 8.08–8.06 (dd, J = 8.39, 2.29 Hz, 1H), 7.48–7.42 (m, 2H), 7.39–7.36 (dd, J = 8.01, 4.58 Hz, 1H), 3.82 (t, J = 4.58 Hz, 4H), 3.21 (s, 2H), 2.62 (t, J =

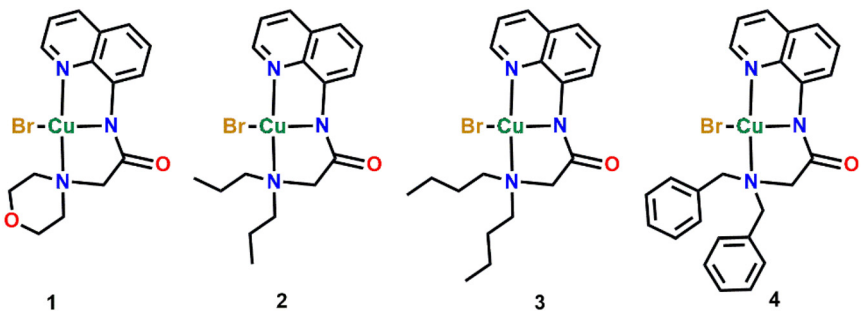

Scheme 1 Copper(II) complexes of aminoquinoline based NN_2 pincer ligands.

4.58 Hz, 4H). ATR, cm^{-1} (Fig. S1†): 1694 cm^{-1} (C═O) and 3265 cm^{-1} (N–H).

2.3.2. 2-Di-*n*-propylamino-*N*-(quinolin-8-yl)acetamide, L2(H). Off-white oil; yield, 90(2)%. ^{1}H NMR (500 MHz, $CDCl_3$, 298 K): δ (ppm) 11.47 (s, 1H), 8.74–8.72 (m, 2H), 8.06–8.04 (dd, J = 8.39, 1.53 Hz, 1H), 7.47–7.41 (m, 2H), 7.36–7.34 (dd, J = 8.01, 4.58 Hz, 1H), 3.23 (s, 2H), 2.51 (t, J = 6.87 Hz, 4H), 1.57–1.49 (m, 4H), 0.89 (t, J = 6.87 Hz, 6H). ATR, cm^{-1} (Fig. S1†): 1676 cm^{-1} (C═O) and 3264 cm^{-1} (N–H).

2.3.3. 2-Di-*n*-butylamino-*N*-(quinolin-8-yl)acetamide, L3(H). Yellow oil; yield, 80(2)%. ^{1}H NMR (500 MHz, $CDCl_3$, 298 K): δ (ppm) 11.54 (s, 1H), 8.83–8.80 (m, 2H), 8.15–8.13 (dd, J = 8.39, 1.53 Hz, 1H), 7.55–7.49 (m, 2H), 7.45–7.42 (dd, J = 8.39, 4.58 Hz, 1H), 3.30 (s, 2H), 2.61 (t, J = 6.87 Hz, 4H), 1.60–1.54 (m, 4H), 1.46–1.38 (m, 4H), 0.89 (t, J = 6.87 Hz, 6H). ATR, cm^{-1} (Fig. S1†): 1680 cm^{-1} (C═O) and 3245 cm^{-1} (N–H).

2.3.4. 2-Di-*n*-benzylamino-*N*-(quinolin-8-yl)acetamide, L4(H). Ligand **L4**(H) was synthesized using a previously reported procedure with slight modifications.[6,7] 2-Bromo-*N*-(quinolin-8-yl)acetamide (1 g, 3.77 × 10^{-3} mol) and three equivalents of dibenzylamine (2.23 g, 11.3 × 10^{-3} mol) were dissolved in acetone and refluxed overnight. The reaction mixture was cooled and subjected to extraction using ethyl acetate followed by brine solution. The organic fraction was dried over sodium sulfate and concentrated under reduced pressure. A silica column was used with a hexane (**4**) : ethyl acetate (**1**) mixture to obtain the pure ligand with a yield of 60(2)% as a white powder. ^{1}H NMR (500 MHz, $CDCl_3$, 298 K) δ (ppm): 11.67 (s, 1H), 9.03 (s, 1H), 8.76–8.73 (m, 1H), 8.20–8.18 (dd, J = 8.20, 1.53 Hz, 1H), 7.67–7.65 (d, J = 6.87 Hz, 4H), 7.54–7.52 (m, 3H), 7.33–7.30 (t, J = 7.25 Hz, 4H), 7.25–7.22 (m, 2H), 3.76 (s, 4H), 3.38 (s, 2H). ^{13}C NMR (125 MHz, $CDCl_3$, 298 K) δ (ppm): 58.89, 59.09, 116.40, 121.59, 121.67, 127.34, 127.41, 128.07, 128.47, 129.22, 134.47, 136.21, 138.17, 138.79, 148.19, 169.99. ATR, cm^{-1} (Fig. S1†): 1676 cm^{-1} (C═O) and 3280 cm^{-1} (N–H).

2.3.5. [Cu(L1)(Br)], 1. Green colour; yield, 75(1)%. Single crystals were obtained by the slow evaporation of a methanol–chloroform solution of **1** in two days. Elemental analysis calcd. for ($C_{15}H_{18}N_3O_3BrCu$): C 41.82, H 3.98, N 9.75; found: C 41.79, H 3.97, N 9.72.

2.3.6. [Cu(L2)(Br)], 2. Green colour; yield, 65(2)%. The crystalline compounds were obtained in methanol solvent. Elemental analysis calcd. for ($C_{17}H_{22}N_3OBrCu$): C 47.73, H 5.18, N 9.82; found: C 47.71, H 5.16, N 9.79.

2.3.7. [Cu(L3)(Br)], 3. Green colour; yield, 66(2)%. The crystalline compounds were obtained in methanol solvent. Elemental analysis calcd. for ($C_{19}H_{26}N_3OBrCu$): C 50.06, H 5.75, N 9.22; found: C 49.96, H 5.73, N 9.19.

2.3.8. [Cu(L4)(Br)], 4. Copper(II) bromide (0.1 g, 4.47 × 10^{-4} mol) was dissolved in methanol. Then ligand **L4**(H) (0.17 g, 4.47 × 10^{-4} mol) was added to the methanolic solution of copper(II) bromide under constant stirring. Following this, triethylamine (TEA, 0.062 mL, 4.47 × 10^{-4} mol) was added to the reaction mixture to remove the amide N–H proton. The reaction continued for 4 h and isolated the green coloured precipitate with a yield of 53(2)%. ATR-IR data (cm^{-1}) (Fig. S2†): 1597 cm^{-1} (C═O), QTOF MS m/z (%) (Fig. S3†): 443.10 (calcd), 443.10 $[Cu(L4)]^+$ (found). Elemental analysis calcd. for ($C_{25}H_{22}N_3OBrCu$): C 57.31, H 4.23, N 8.02; found: C 57.22, H 4.21, N 7.99.

2.4. Single-crystal X-ray diffraction studies

By careful examination under an optical microscope, fine single crystals suitable for X-ray diffraction were chosen from the mother liquor of complex **1**. Single crystals were mounted using a fibre loop and optically centered. The automatic cell determination routine was employed to collect reflections (24 frames at three different orientations of the detector) and the APEX3-SAINT program was used for determining the unit cell parameters.[30]

The data were corrected for Lorentz-polarization effects. Semiempirical absorption correction (multi-scan) based on symmetry-equivalent reflections was applied using the SADABS program.[31] The structures were solved by direct methods and refined by full-matrix least-squares, based on F^2 using SHELX-2018 software package2 and the WinGX program.[32] The crystallographic details of the data collected for **1** are given in Table 1.

2.5. MTT assay

The MTT [3-(4,5-dimethylthiazol-2-yl)-2,5-diphenyltetrazolium bromide] assay can discern the metabolic activity using the colorimetric technique. In the presence of viable cells, MTT turns into purple formazan from yellow colour.[33,34] Once the cell culture was trypsinized, a medium containing 10% fetal bovine serum (FBS) was used to adjust the cell count to 1 × 10^5 cells per mL. Then, they were filled in 96-well microliter plates

Table 1 Crystallographic data for complex **1**

	1
Empirical formula	$C_{15}H_{18}BrCuN_3O_3$
Formula weight, g mol^{-1}	431.77
Crystal habit, colour	Block, green
Crystal system	Monoclinic
Crystal size, mm	0.042 × 0.030 × 0.025
Space group	$P2_1/n$
a, Å	7.9149(8)
b, Å	18.466(2)
c, Å	11.1514(11)
α, °	90
β, °	94.607(7)
γ, °	90
V (Å^3)	1624.6(3)
Z	4
ρ_{calcd}/mg m^{-3}	1.765
F(000)	868
Temperature (K)	298(2)
No. of reflections collected	9012
Independent reflections	2055 [R(int) = 0.1366]
Radiation (Mo-Kα)/Å	1.54178
Goodness-of-fit on F^2	1.203
Number of refined parameters	214
R_1/wR_2[$I > 2\sigma(I)$][a]	R_1 = 0.1300, wR_2 = 0.3196
R_1/wR_2 (all data)	R_1 = 0.2503, wR_2 = 0.4030

[a] $R_1 = [\sum(||F_o| - |F_c||)/\sum|F_o|]$; $wR_2 = \{[\sum(w(F_o^2 - F_c^2)^2)/\sum(wF_o^4)]\}^{1/2}$.

in such a way that each well contained 50000 cells. A partial monolayer was formed after 24 h. This monolayer was rinsed with the medium and compounds dissolved in DMSO were added in serial dilutions from 20 μM to 0 μM. Furthermore, it was incubated for 24 h. Then, 100 μL of 5 mg per 10 mL MTT in PBS (phosphate buffered saline) was distributed in each well and incubation was continued for 4 h. Following the removal of the supernatant, 100 μL of DMSO was introduced to solubilize the formazan. The absorbance of this solution was determined using a microplate reader (Tecan plate reader) at 590 nm. The following formula was used to determine the extent of cell growth inhibition:

$$\%\text{Inhibition} = 1 - \frac{\text{Absorbance of the sample}}{\text{Absorbance of the control}} \times 100 \quad (1)$$

Furthermore, the dose–response curve between different concentrations of compounds against the percentage inhibition was able to obtain the half-maximal inhibitory concentration (IC_{50}). The IC_{50} was computed using GraphPad Prism 6 (GraphPad, San Diego, CA, USA). The IC_{50} values are calculated based on the mean of the triplicate absorptions. In addition, mechanistic studies were carried out for complex **1** against A549 cells due to its elevated activity compared to other complexes.

2.6. Acridine orange (AO)–ethidium bromide (EB) staining

Cells treated with **1** were examined for apoptosis using a dual AO–EB fluorescence staining method.[35–37] In a nutshell, 4000 cells per well in 24 well plates were processed with **1** at the IC_{50} concentration and incubated for 24 h. The staining solution containing AO and EB at a concentration of 100 g mL^{-1} was added to each well at a volume of 500 μL after 24 h of incubation. The results were observed through a fluorescence microscope.

2.7. Flow cytometry

Annexin V-FITC/PI staining is considered as a sophisticated technique that can distinguish cells of viable, apoptotic, and necrotic features.[38–40] Once 10^5 cells per well were cultured under incubation for 24 h in a 6-well plate, they were treated with **1** at the IC_{50} concentration. The cells were trypsinized, and after 24 h of incubation, they were rinsed with PBS and dyed with Annexin V-FITC/PI in accordance with the instructions on the Annexin V-FITC apoptosis detection kit. The cells that have not undergone treatment with **1** were treated as the control. Furthermore, the extent of cell death was evaluated using a SYSMEX flow cytometer (Japan) and analyzed using FlowJo software.

2.8. Determination of ROS

Carboxy-H_2DCFDA (2′,7′-dichlorodihydrofluorescein diacetate) is normally non-fluorescent. Once ROS is present, it oxidises to show green fluorescence.[41–43] A fresh stock solution of carboxy-H_2DCFDA was prepared in sterile 100% ethanol right before use. After 24 hours, **1** at the IC_{50} concentration was treated with carboxy-H_2DCFDA (1 μM) in a regular culture medium with reduced serum (2%) and incubated for 30 minutes. The medium containing carboxy-H_2DCFDA was removed and washed with PBS twice. A fluorescence microscope was used to examine the cells.

2.9. Determining the mitochondrial membrane potential (MMP) by JC-1 staining

Roughly 5×10^5 cells per mL were cultured on coverslips in a 6-well culture plate and incubated for 8 h.[44–46] After 24 h of incubation with **1** at the IC_{50} concentration, 1–10 μM of JC-1 dye was added to the cell culture medium as a working stock solution and the plates were incubated (15–30 min). The dead cell percentage was immediately observed under a fluorescence microscope.

2.10 Lipophilicity and Stability studies

The lipophilicity was determined by the shake-flask method using a pre-saturated 1-octanol-water solution which is detailed in the ESI.† [47] The stability of the complexes was calculated according to their decay in DMSO and FBS using UV-vis spectroscopy. The absorption spectra of compounds dissolved in DMSO and 5% DMSO in FBS were recorded at 0 h and after 24 h. The percentage of decay was calculated from the differences in the absorption of both spectra.

2.11. Molecular docking

The interaction of complexes **1–4** with complex I of mitochondria was performed using AutoDock Vina.[48] The protein structure, 5XTD, was obtained from the Protein Data Bank. The active site was included completely by creating grid box dimensions of 46 Å × 66 Å × 74 Å and the same was used for all the complexes. The Gaussian 09 software package at the B3LYP level of theory and the basis sets 6-31G for C, H, O, and N and LANL2DZ for the metal centre were used to optimize the geometry of the complexes.[49] The output was visualized and analysed using Autodock tools 1.5.7 and Discovery Studio.[50]

3. Results and discussion

3.1. Synthesis and characterization of ligands and copper(II) complexes

As per the literature method, ligands **L1**(H), **L2**(H), **L3**(H) and **L4**(H) were obtained by reacting 2-bromo-*N*-(quinoline-8-yl) acetamide with morpholine, diisopropylamine, dibutylamine, and dibenzylamine, respectively.[6,7] Then, by stirring a methanolic solution of an equivalent amount of ligand, $CuBr_2$, and triethylamine, copper(II) complexes **1–4** were synthesized as reported.[7] The isolated compounds were characterized using advanced analytical techniques. For instance, the removal of a N–H peak during complex formation was clearly visible from the disappearance of the peak around 3245–3280 cm^{-1} in the ATR-IR spectra of **4** compared to the corresponding ligand **L4**(H). This observation was similar for **1–3** and **L1**(H)–**L3**(H).[7] Mass spectrometry also revealed the formation of **4**. A square planar coordination geometry of the copper(II) centre of **1–4** in

solution was indicated by a highly intense peak around 356–364 nm and a peak corresponding to a d–d transition around 631–655 nm in the UV-visible spectra. Complex **4** was observed with *g*-tensors ($g_{||}$ = 2.293 and $g_{\perp}$ = 2.039) and coupling constants ($A_{||}$ = 194 × 10^{-4} cm^{-1}) gained from the axial symmetry EPR spectra that match very well with the recently reported EPR spectra of **1–3**.[7] Furthermore, structural characterization of complex **1** by single-crystal X-ray crystallography revealed a distorted square pyramidal geometry that can be formulated as [Cu(L1)Br(H_2O)].

3.2. Infrared spectra of 1–4 with L1(H)–L4(H)

Ligands **L1**(H)–**L4**(H) exhibited two major peaks around 3245–3280 and 1676–1694 cm^{-1} in the functional group region, which are assigned to N–H (**L1**(H), 3265 cm^{-1}; **L2**(H), 3264 cm^{-1}; **L3**(H), 3245 cm^{-1}; and **L4**(H), 3280 cm^{-1}) and C=O (**L1**(H), 1694 cm^{-1}; **L2**(H), 1676 cm^{-1}; **L3**(H), 1680 cm^{-1}; and **L4**(H), 1676 cm^{-1}) groups. Upon complexation with $CuBr_2$ in the presence of TEA, the N–H peak completely disappeared in **1–4**, revealing N^- (amido) coordination to the copper centre (Fig. S1 and S2†). Furthermore, the decrease in C=O stretching frequencies (1587–1597 cm^{-1}) was also noticed after complexation, indicating that the electron density localized more towards the copper centre. All these results were in concordance with the data recently reported by us.[7]

3.3. Electronic properties of complexes

Complexes **1–4** showed two peaks in the UV-visible spectra in methanol at room temperature. The observed highly intense peaks at around 356–364 nm (**1**, 356 nm (ε, 4610 M^{-1} cm^{-1}); **2**, 357 nm (ε, 4095 M^{-1} cm^{-1}); **3**, 357 nm (ε, 4755 M^{-1} cm^{-1}); and **4**, 364 nm (ε, 4070 M^{-1} cm^{-1})) are assigned to the charge transfer transition from the ligand to the copper(II) centre (LMCT) (Fig. 1). The other broad peaks at around 631–655 nm (**1**, 655 nm (ε, 145 M^{-1} cm^{-1}); **2**, 631 nm (ε, 130 M^{-1} cm^{-1}); **3**, 633 nm (ε, 160 M^{-1} cm^{-1}); and **4**, 647 nm (ε, 135 M^{-1} cm^{-1})) with a low intensity are assigned to the d–d transition ($^2B_{1g}$ → ^2E_g in square planar copper(II) complexes).[7,51]

The frozen EPR spectra of complex **4** exhibit a well-refined axial symmetry (Fig. 2), with *g*-tensors $g_{||}$ = 2.293 and $g_{\perp}$ = 2.039 and coupling constants ($A_{||}$ = 194 × 10^{-4} cm^{-1}), which were comparable to those reported for complexes **1–3** ($g_{||}$ = **1**, 2.285; **2**, 2.283; and **3**, 2.274 and $g_{\perp}$ = **1**, 2.042; **2**, 2.039; and **3**, 2.033) and coupling constants ($A_{||}$ in × 10^{-4} cm^{-1} = **1**, 197; **2**, 197; and **3**, 197).[7] In addition to low $g_{||}$ and high $A_{||}$ values, it is observed that the *f* quotient (118 cm^{-1}) falls within 105–135 cm^{-1}, which suggests that the planar nature of complex **4** is similar to the other complexes **1–3**.[7,52] Moreover, the square-based geometry of the complexes was perceptible from the $g_{||} > g_{\perp}$ values, which indicates that $d_{x^2-y^2}$ is the ground state.[53]

3.4. Molecular geometry of 1

The molecular structure of complex **1** is shown in Fig. 3 with the atom numbering scheme, principal bond lengths and bond angles provided in Table 2. It was observed that **1** exhibits a distorted square pyramidal geometry with a monoclinic crystal system and the $P2_1/n$ space group. The tridentate chelating ligand is coordinated in a facial fashion towards the copper(II) centre with the nitrogen atoms of quinolyl, amido and morpholine, along with a bromine atom (Br) and a water molecule (O(3)). This water molecule (O(3)) might be present in the solvent of crystallization, revealed by the lack of a peak corresponding to OH in the IR spectra of **1** (Fig. S2† (**1**)). Moreover, the coordination around the copper(II) of **1** with bond angles ranging from 91.7° to 110.4° that deviate from the ideal square pyramidal angles of 90° and 180° was observed. Here, the coordination around copper gives a trigonality index

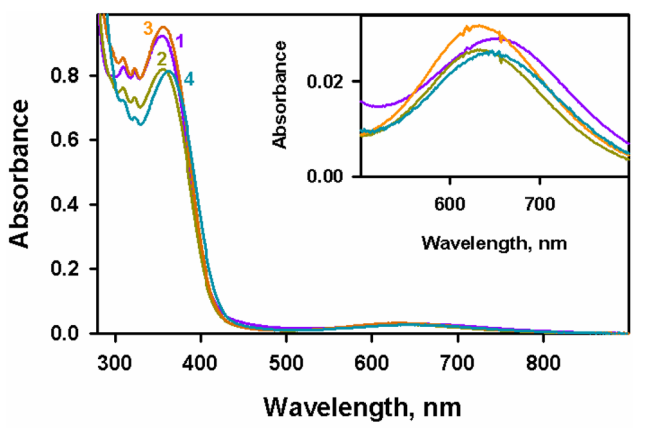

Fig. 1 UV-visible spectra of **1–4** (2 × 10^{-4} M) recorded in methanol at 298 K.

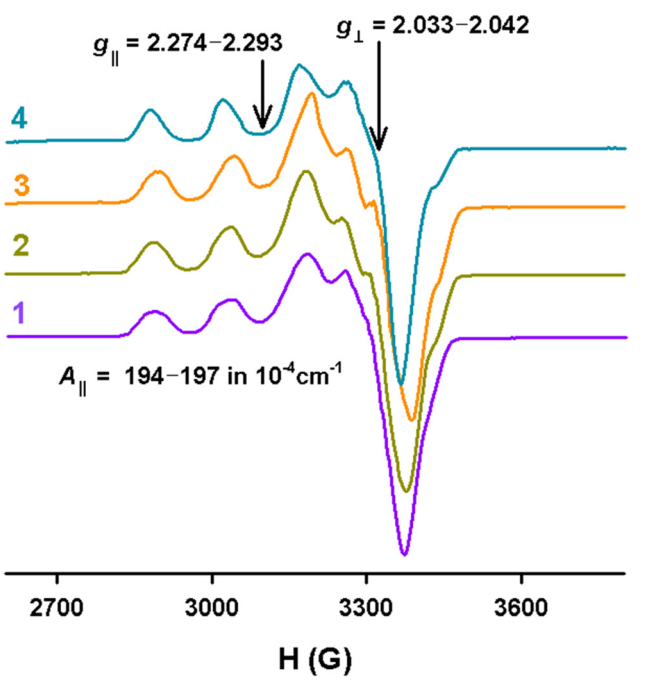

Fig. 2 A comparison of the frozen EPR spectrum of **4** with that of **1–3** in DMF : methanol (4 : 1 v/v) measured at 100 K.[7]

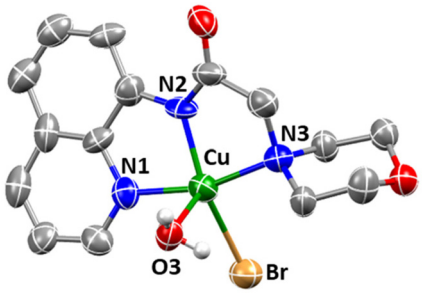

Fig. 3 ORTEP diagram of **1** showing 30% probability of thermal ellipsoids, and the labelling scheme of the atoms. Hydrogen atoms in the chelating ligands are omitted for clarity.

Table 2 Selected bond lengths [Å] and bond angles [°] of **1**

	Bond lengths/Å
Cu–N(1)	2.004(16)
Cu–N(2)	1.909(17)
Cu–N(3)	2.070(16)
Cu–Br	2.456(5)
Cu–O(3)	2.251(16)
	Bond angles [°]
N(1)–Cu–N(2)	80.2(9)
N(1)–Cu–N(3)	164.0(8)
N(2)–Cu–N(3)	83.8(8)
N(1)–Cu–Br	95.7(6)
N(2)–Cu–Br	152.0(6)
N(3)–Cu–Br	98.1(6)
N(1)–Cu–O(3)	91.7(6)
N(2)–Cu–O(3)	110.4(7)
N(3)–Cu–O(3)	94.5(6)
O(3)–Cu–Br	97.3(5)

(τ_5) of 0.2 ($\tau_5 = (\beta - \alpha)/60$, where α = N(2)–Cu(1)–Br = 152° and β = N(1)–Cu(1)–N(3) = 164°).[54] As expected, the bond length of Cu(II)–$N_{quinoline}$ (N(1)) is shorter than the bond distance of Cu(II)–$N_{morpholine}$ (N(3)) due to the sp^2 hybridized quinoline ring.

Very recently, complexes **2** and **3** have been reported with a square planar geometry that is slightly distorted and crystallize with the space groups *C*2/*c* and $P2_1/n$, respectively, in a monoclinic system.[7] Upon examining the bond parameters of **2** and **3**, it is found that the bond angles and bond lengths are comparable to those of complex **1**. It should be noted that in all complexes (**1–3**), the Cu–N_{amine} (2.070(16)–2.0901(16) Å) bond is lengthier than the Cu–$N_{quinoline}$ (2.004(16)–2.0457(16) Å) bond, which is consistent with the sp^3 and sp^2 hybridizations, respectively. Moreover, these complexes deviate from their ideal structures with trigonality indexes of τ_5 = 0.2 for **1**, τ_4 = 0.16 for **2**, and 0.24 for **3**. Also, the distorted square pyramidal coordination of **1** was found to be similar to that of the recently reported zinc(II) complex [Zn(L1)Cl(H_2O)] with a τ_5 value of 0.257.[6]

3.5. Activity of 1–4 against lung (A549) and breast (MCF-7) cancer cell lines

3.5.1. The impact of 1–4 on cellular viability. The effect of complexes **1–4** on A549 and MCF-7 cell lines was examined from the diagrams of percentage viability (Fig. 4A and S4†), which clearly demonstrate the complex's enhanced activity with an increase in concentration. All the complexes exhibited a promising antiproliferative effect against A549 (IC_{50} (μM): **1**, 8; **2**, 13.95; **3**, 13.85; and **4**, 20) (Table S1†) and MCF-7 (IC_{50} (μM): **1**, 15; **2**, 17.55; **3**, 15.75; and **4**, 19.35) cancer cells (Fig. 4B). The most promising cytotoxic effect was shown by **1** against A549 cells (IC_{50} = 8 μM). The activity of **1–4** is clearly visible from the culture morphology phase images provided in Fig. 5 and S5, S6.† Since the MTT assay was performed by dissolving compounds in DMSO and the biological medium of FBS, the stability of complexes was checked in both using UV-vis spectroscopy techniques. This shows that approximately 94–99.5% of complexes remained without any decay in DMSO (Fig. S7†) and 89–91% in FBS (Fig. S8†). It should be noted that in the case of **4** in FBS, the stability could not be calculated due to the formation of turbidity after 24 h (Fig. S8†). To understand more about the importance of this copper complex, the cytotoxicity of the corresponding ligand **L1**(H) was also examined (Fig. S9†). Almost a 10-fold increase in cytotoxicity is observed after the complexation of **L1**(H) (IC_{50} (μM) = A549, 77.65; MCF-7, 77.52) with copper (Fig. S10†). The selectivity and excellent cytotoxicity of **1** against A549 cell lines made us proceed with further mechanistic studies. Moreover, the non-toxic nature of **1** against healthy cells was identified by treating it against a normal L929 fibroblast cell line (IC_{50} > 1000 μM) (Fig. S11†). It is important to note that the IC_{50} value of cisplatin against A549 cells is 29.25 μM under identical conditions, revealing that the present copper(II) complexes could be beneficial for overcoming the limitations of Pt-based chemotherapeutics.[6] It is also evident that **1–4** show good activity compared with the reported copper complexes of similar ligand architectures.[25–29] For example, the selected pincer-type copper complexes [Cu(MQA)(OAc)] where MQA = L-methionine-*N*′-8-quinolylamide, [$CuCl_2$(thiophen-2-yl-terpy)] where terpy = 2,2′:6′,2″-terpyridine, [Cu(Me)(*N*-TP)(PF_6)], [Cu(Et)(*N*-TP)(PF_6)], and [Cu(iPr)(*N*-TP)(PF_6)] where *N*-TP = *N*-aryl-1,3,5-triaza-7-phosphaadamantane, [Cu(L)Cl](ClO_4), and [Cu(L)Br_2] where L = 2-((quinolin-8-ylimino)methyl)pyridine exhibit IC_{50} (μM) values of 1, 4.2, 3.92, 3.14, 2.35, 0.90, and 0.43, respectively, against A549 cells.[25–28] It should be noted that, even though these complexes have lower IC_{50} values than the present complex **1** (incubation time: 24 h), their incubation time is high (≥48 h).

Similarly, complexes [Cu(κ^3-L)(Cl_2)]·3H_2O, [Cu(κ^3-L)($SCN)_2$], and [Cu(κ^3-L)($ClO_4)_2$], where L = 2,6-bis[[(4-bromophenyl)thio]methyl]pyridine, show results (IC_{50} = 12.38–14.98 μM) comparable to the present complexes against A549 cells under incubation for 48 h.[29] Other complexes [Cu(CMQA)(H_2O)] where CMQA = *N*-carboxymethyl-L-methionine-*N*′-8-quinolylamide, [$CuCl_2$(1-methyl-1*H*-pyrrol-2-yl-terpy)], and [$CuCl_2$(R-dtpy)] where R = furan-2-yl, thiophen-2-yl, 1-methyl-1*H*-pyrrol-2-yl and dtpy = 2,6-di(thiazol-2-yl)pyridine show less activity against A549 cells (IC_{50} = 64.3–100 μM) compared to the present complexes **1–4**.[25,27]

In a similar way, comparing the reported activity of copper pincer complexes against MCF-7 revealed that [Cu(Me)(*N*-TP)(PF_6)], [Cu(Et)(*N*-TP)(PF_6)], [Cu(iPr)(*N*-TP)(PF_6)], [Cu(L)Cl](ClO_4),

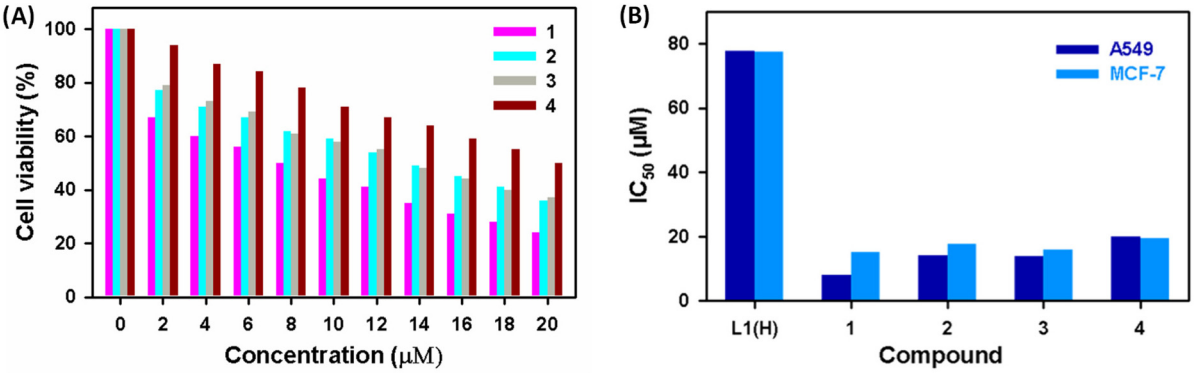

Fig. 4 (A) Viability of A549 under complex **1** and (B) IC_{50} values of ligand **L1**(H) and complexes **1–4** effective against A549 and MCF-7 cancer cell lines.

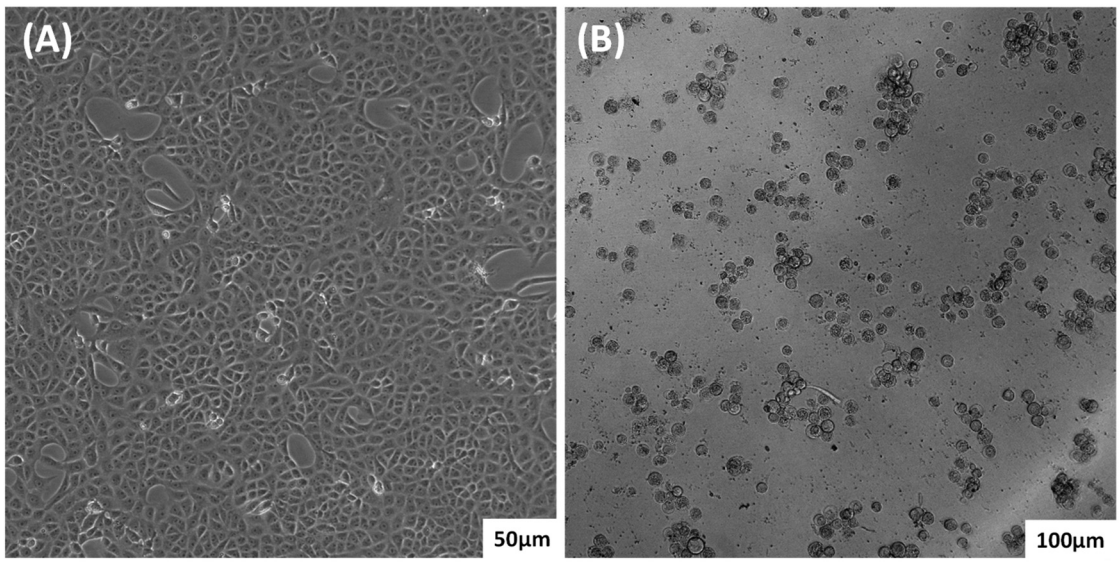

Fig. 5 Phase images of (A) control A549 cells and (B) A549 cells treated with **1**.

and $[Cu(L)Br_2]$ have IC_{50} values in between 0.46 and 8.41 μM, at an incubation time of 48 h. At the same time, it is observed that complexes $[CuCl_2$(R-terpy)] and $[CuCl_2$(R-dtpy)] where R = furan-2-yl, thiophen-2-yl, and 1-methyl-1*H*-pyrrol-2-yl are less active than **1–4** with IC_{50} values ranging between 43 and 100 μM against MCF-7 at 48 h of incubation.[27] Very recently, we have reported the anticancer activity of zinc complexes of ligands **L1**(H)–**L3**(H) against A549 and MCF-7 cells and found that the IC_{50} values range from 16.35 to 17.95 and 33.35 to 40 μM, respectively.[6] This diminished activity of zinc analogues indicates the supremacy of copper complexes in cancer therapy. Moreover, among the copper(II) complexes, **1** of **L1**(H) has the highest activity but in the case of zinc(II) complexes, **3** of **L3**(H) has the best activity. From this, it is understood that the ligand system also affects the activity along with the choice of metal ions.

3.5.2. Complex 1 induced apoptosis in A549 cells: detection and quantification. The cytological changes that occurred in A549 cells treated with **1** using the AO–EB staining assay were examined.[28] As shown in Fig. 6A, the viable cells are observed as well-organized structures having nuclei with green fluorescence. Other morphological changes were observed after treating the cells with **1** as shown in Fig. 6B. Here, vivid green patches of perinuclear chromatin, red fluorescent nuclei, and swollen red luminous nuclei without chromatin rupture are an indication of early apoptotic, late apoptotic, and necrotic cells, respectively.

Furthermore, the quantification of apoptosis in A549 cells induced by **1** was marked using flow cytometry. A549 cells treated with **1**, at the IC_{50} concentration, showed a different extent of cell death compared with the control, as shown in Fig. 7. This resulted in 2.61% (Q3) of cells under apoptosis, 23.3% (Q2) of cells in the late apoptotic stage, and 5.47% (Q1) of necrotic cells (Fig. 7). The impact of **1** is clearly visible by comparing the results with that of the control (Q2 = 0.076%, Q3 = 0.41%, and Q1 = 3.1%). These findings altogether revealed that apoptosis is the primary mechanism by which the complex caused cell death. Similarly, the reported terpyri-

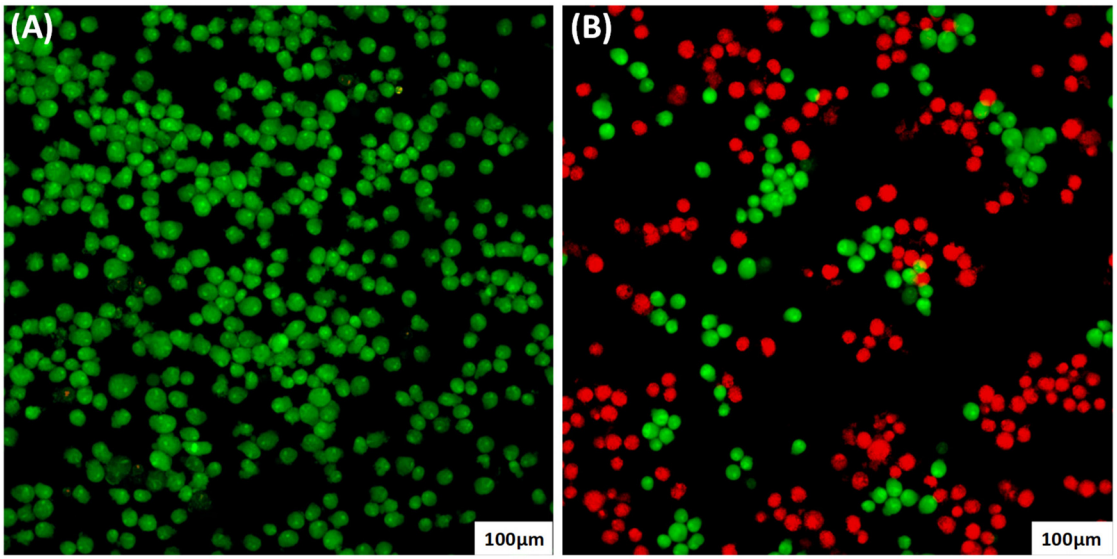

Fig. 6 AO–EB stained (A) A549 cells and (B) A549 cells treated with **1** at the IC_{50} concentration.

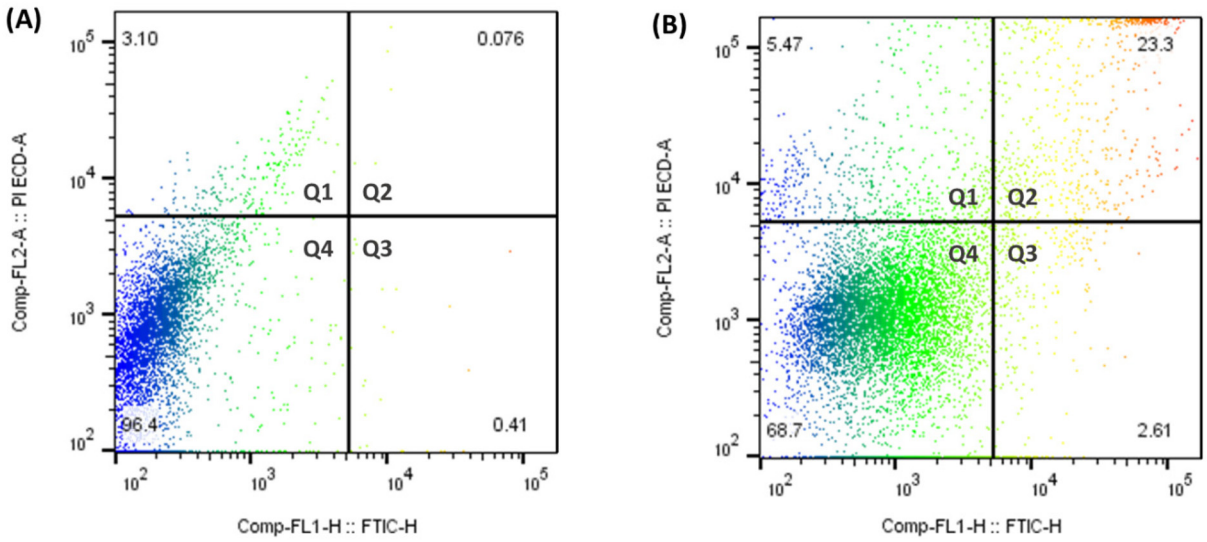

Fig. 7 Annexin V-FITC/PI staining in A549 cells: (A) control and (B) after being treated with **1** at the IC_{50} concentration.

dine based copper(II) pincer complexes were active against A549 and MCF-7 cell lines and were able to induce apoptosis in A549 cells.[27] Similarly, the reported zinc(II) complex of **L3** (H) had a slightly low percentage of cells under apoptotic (1.37%), late apoptotic (21.4%), and necrotic (4.94%) cells compared to that of the present copper(II) complexes in the flow cytometry experiment.[6]

3.5.3. Root cause of apoptosis in A549 cells by 1. The primary mechanism of anticancer activity by copper complexes involves excessive ROS production by which DNA/RNA can be oxidized or lipid peroxidation can progress. The redox process mediated by the potential reduction of the metal centre Cu(II)/Cu(I) might lead to the formation of oxidative species.[55] Intracellular ROS levels in A549 cells and excess ROS formation by **1** were compared using the H_2DCFDA staining technique. Here, it is observed that the cells treated with **1** and H_2DCFDA showed more intense fluorescence than that of the control as in previous reports (Fig. 8).[56] This observation is an outcome of the availability of excess ROS in the complex treated cells. For instance, the cyclometalated Cu(I) pincer complexes with phosphaadamantane derivatives also induced excess ROS generation that led to apoptosis in A549 cells.[28]

ROS-induced damage is more prominent in mitochondrial DNA than nuclear DNA.[57] The JC-1 assay is a very effective way to find depolarization of the mitochondrial membrane. Once the JC-1 dye enters the mitochondria of a healthy cell, it emits red fluorescence (~590 nm) of J-aggregates in healthy cells and green fluorescence (~525 nm) of their monomeric form in

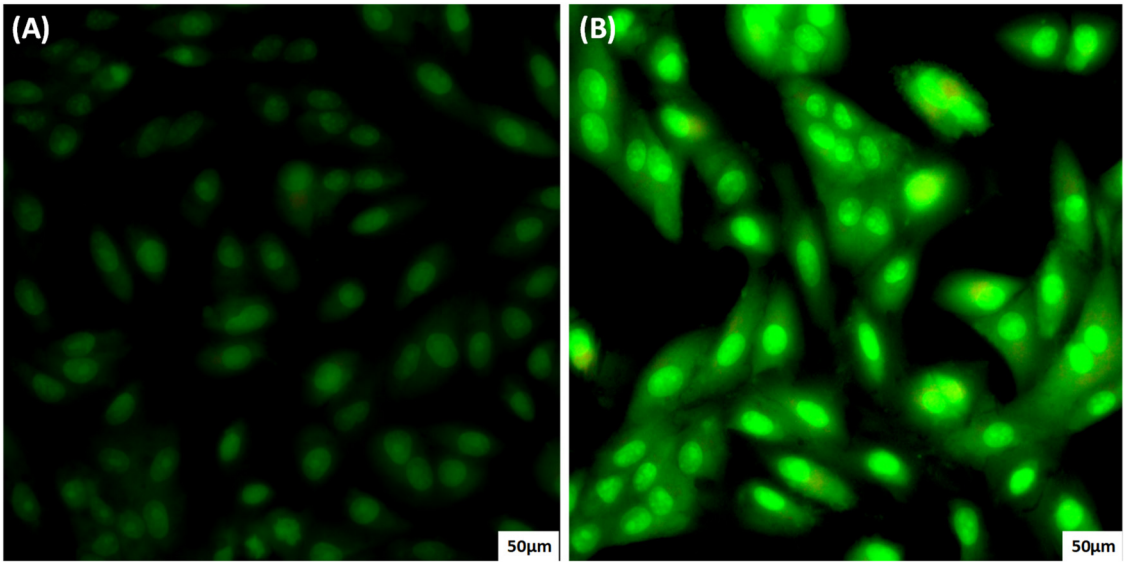

Fig. 8 H_2DCFDA stained A549 cells: (A) control and (B) after being treated with **1** at the IC_{50} concentration.

unhealthy cells. Fig. 9 explains the change in the MMP. Moreover, this change is due to the increased production of ROS which causes membrane permeabilization and results in the release of cytochrome c.[58] This change in the MMP is an indication of the initial phase of apoptosis.[59] Moreover, it is observed that the recently reported zinc(II) complex of **L3**(H) promotes the production of excess ROS and changes in the MMP.[6] However, the higher activity of the present copper complexes **1–3** than their zinc analogues might be due to the inherent redox-active nature of copper.

As alluded to above, the ROS formation and the change in the MMP were confirmed experimentally, and thus we propose the mechanism of anticancer activity of **1–4** with the generation of ROS in mitochondria by perturbing the function of complex I as reported earlier.[60–62] Being the first enzyme of the respiratory chain, complex I has a vital role in cellular energy production.[63] This is possible only if **1–4** are capable of anchoring near complex I. To support this postulate, we examined molecular docking with complex I of PDB ID: 5XTD with our copper complexes.[64]

Interestingly, we found that **1** binds very near to the flavin mononucleotide (FMN) site of complex I (Fig. 10A); conversely, **2–4** bind away from this site with docking scores of −7.3, −6.6, −8.2, and −8.4 kcal mol^{-1}, respectively (Fig. S12–S14†) under the same grid box sizes.[65] Complex **1** binds to Gly350 (2.32 Å) and Leu349 (2.86 Å) amino acids through a strong hydrogen bonding. In complex **2**, the donor–donor bond between His376 and the amide nitrogen is very strong with a distance

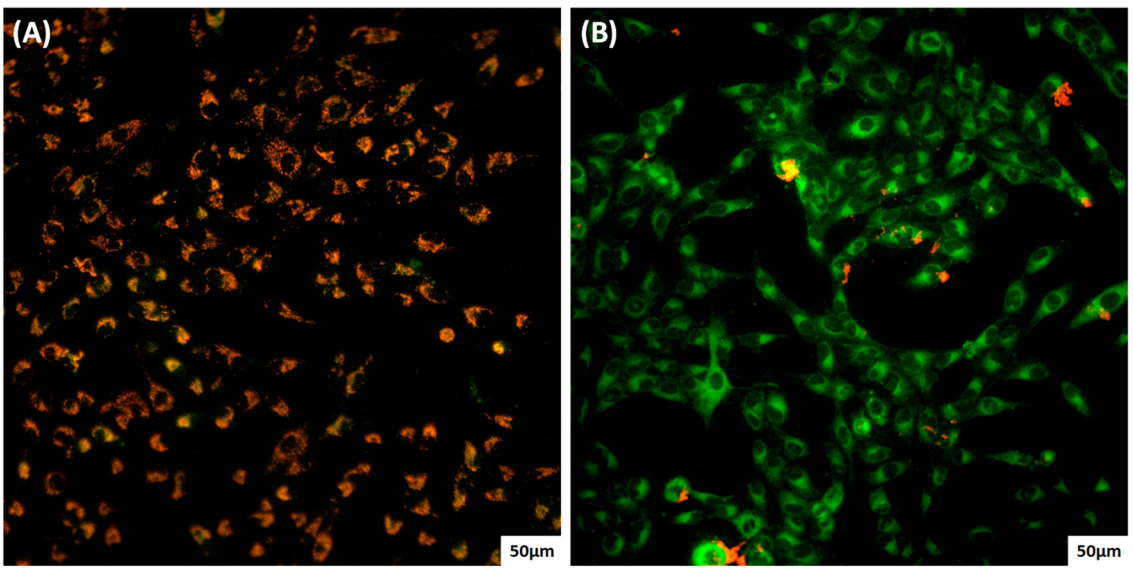

Fig. 9 JC-1 staining assay of A549 cells: (A) control and (B) after being treated with **1** at the IC_{50} concentration.

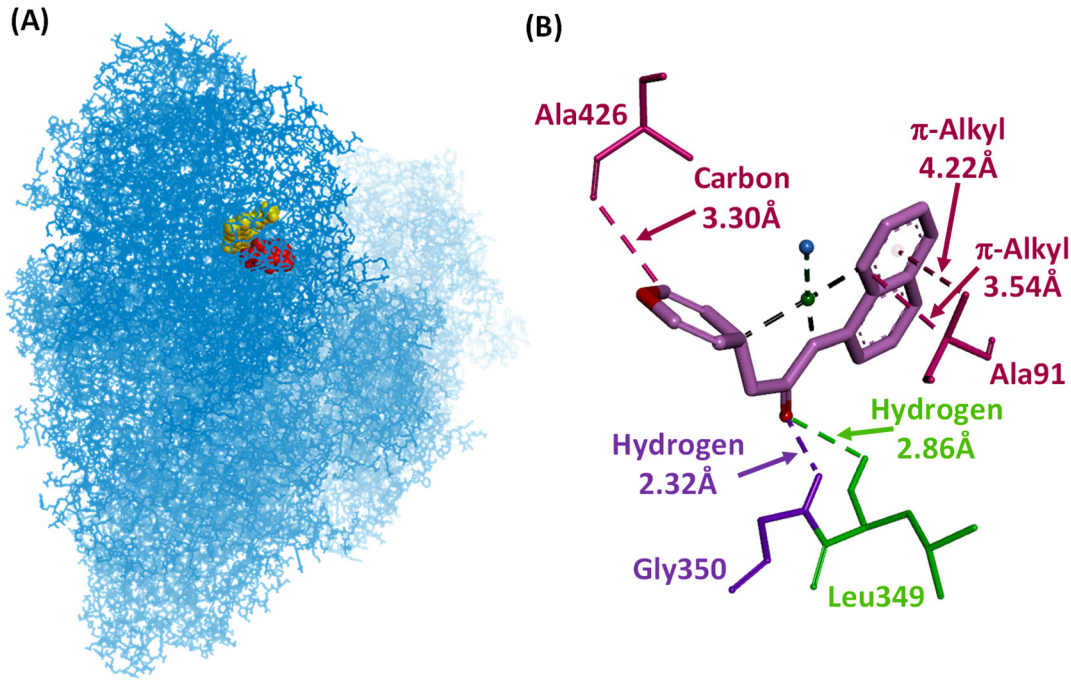

Fig. 10 (A) Molecular docked conformation and (B) interactions of **1** at the active site of 5XTD.

of 2.90 Å. Complex **3** interacted with His74 and Ala76 much more strongly with bond distances of 3.58 Å (carbon) and 3.86 Å (alkyl), respectively. A π–π stacking interaction (3.80 Å) was observed with **4** and His736. In a similar way, the interaction of **4** with Val174 was observed with two strong π–sigma interactions with distances of 3.88 and 3.95 Å. This indicates that **1–4** can interact with complex I of mitochondria and possibly inhibit the activity. Specifically, the strong binding of **1** near the FMN site compared to the other complexes **2–4** might be the reason for its enhanced anticancer activity.

Overall, complexes **1–4** exhibit promising activity against A549 and MCF-7 cell lines. Mechanistic investigation reveals that the cell death of A549 is induced by the most active complex **1** because of the excess production of ROS in the mitochondria and thereby apoptosis. The observation is well supported by experimental and *in silico* studies.

3.6. Lipophilicity analysis

Complex **4** and the corresponding ligand **L4**(H) were found to have a partition coefficient, P (or $\log K_{ow}$), with values of 3.14 and 10.04, respectively, determined by the shake flask method.[47] Compounds **4** and **L4**(H) were found to be highly lipophilic compared to the other complexes **1**, −0.51; **2**, 1.07; and **3**, 1.83 and ligands **L1**(H), 2.71; **L2**(H), 0.67; and **L3**(H), 0.55.[6,7] It should be noted that **1** has a slightly hydrophilic nature and shows the best activity. At the same time, **4** has higher lipophilicity which might not be good for a drug (Fig. S15†). This indicates how the lipo–hydro balance matters for drug molecules. In the present compounds, it is seen that the comparatively highly lipophilic ligands are less active than the copper complexes. The lipophilicity–anticancer activity correlation of the present complexes is useful in the future to design better metal complexes in this field. Moreover, the formation constant (K_f) of complexes **1–4** was calculated in methanol (Fig. S16†). The K_f value of **4** ($K_f = (5.14 \pm 0.97) \times 10^5$ M^{-1}) compared to those of the other complexes **1–3** is in the order **4** < **1** [$(6.21 \pm 4.68) \times 10^5$] < **2** [$(7.19 \pm 2.42) \times 10^7$] < **3** [$(5.50 \pm 3.86) \times 10^9$].[7] The order of formation constant in methanol is concordant with the lipophilicity values, where the most hydrophobic **4** has the lowest K_f value.

4. Conclusion

Currently, growing interest in biological applications of pincer-type metal complexes proves that they can act as drugs with enhanced anticancer activity. To attain such activity, a series of 8-aminoquinoline based pincer ligands and their copper(II) complexes **1–4** were synthesized, characterized and studied for their anticancer activity. The complexes were very efficient against A549 lung and MCF-7 breast carcinoma cells. Interestingly, **1** was very selective against lung cancer cells with an IC_{50} value of 8 μM and it is noteworthy that it showed no toxicity against the normal fibroblast cell line L929 (IC_{50} > 1000 μM). Furthermore, the involvement of ROS in the mechanism of anticancer activity of **1** was determined by carboxy-H_2DCFDA staining. Moreover, the mechanism of cell death was found to be apoptosis using the AO–EB staining assay, and through flow cytometry, it is calculated to be 25.91%. The depolarization of the MMP observed by JC-1 marking indicated elevated ROS production in the mitochondria. Furthermore, the most probable mechanism was found to be the pertur-

bation in the function of complex I of mitochondria by *in silico* studies. Overall, the studies give promising results to extend complex **1** to clinical applications.

Author contributions

Athulya Das: data curation, formal analysis, investigation, resources, software, visualization, writing – original draft, and writing – review & editing. Muniyandi Sankaralingam: conceptualization, formal analysis, funding acquisition, investigation, methodology, project administration, resources, software, supervision, validation, visualization, writing – original draft, and writing – review & editing.

Data availability

The data supporting this article have been included as part of the ESI.†

Crystallographic data for **1** have been deposited at the repository namely CCDC under 2311348 and can be obtained from **https://www.ccdc.cam.ac.uk/data_request/cif** or by emailing data_request@ccdc.cam.ac.uk.

Conflicts of interest

There are no conflicts to declare.

Acknowledgements

MS sincerely acknowledges the Science and Engineering Research Board (SERB) for the CRG grant (CRG/2023/002850). MS and AD sincerely thank the Department of Science and Technology, New Delhi, for awarding the DST-Inspire Faculty research grant (IFA-17-CH286) and the DST-Inspire Fellowship (IF-170136), respectively. The authors thank DST SAIF-IITM for helping with single crystal XRD analysis. We also thank the Department of Chemistry IITM for recording mass spectra. We would like to thank Prof. M. Sankar and his student Mr. Rajesh Kumar for allowing us to record the EPR spectra. We also thank NIT Calicut for the NMR (CMC) and HPC (CCMS) facilities and Thasnim P Mohammed, a PhD Scholar under the guidance of Dr MS in BBICL, for optimizing the geometries. We are pleased to thank the Biome Live Analytical Centre, Karaikudi, for anticancer studies.

References

1 WHO, Cancer. **https://www.who.int/health-topics/cancer#tab=tab_1**, accessed 17.03.2023.
2 S. Sen, M. Won, M. S. Levine, Y. Noh, A. C. Sedgwick, J. S. Kim, J. L. Sessler and J. F. Arambula, Metal-Based Anticancer Agents as Immunogenic Cell Death Inducers: The Past, Present, and Future, *Chem. Soc. Rev.*, 2022, **51**, 1212–1233.
3 D. Hernández-Romero, S. Rosete-Luna, A. López-Monteon, A. Chávez-Piña, N. Pérez-Hernández, J. Marroquín-Flores, A. Cruz-Navarro, G. Pesado-Gómez, D. Morales-Morales and R. Colorado-Peralta, First-Row Transition Metal Compounds Containing Benzimidazole Ligands: An Overview of Their Anticancer and Antitumor Activity, *Coord. Chem. Rev.*, 2021, **439**, 213930.
4 A. Das, A. Rajeev, S. Bhunia, M. Arunkumar, N. Chari and M. Sankaralingam, Synthesis, Characterization and Antimicrobial Activity of Nickel(II) Complexes of Tridentate N3 Ligands, *Inorg. Chim. Acta*, 2021, **526**, 120515.
5 (*a*) A. Das, T. P. Mohammed, R. Kumar, S. Bhunia and M. Sankaralingam, Carbazole Appended *Trans*-Dicationic Pyridinium Porphyrin Finds Supremacy in DNA Binding/Photocleavage over a Non-Carbazolyl Analogue, *Dalton Trans.*, 2022, **51**, 12453–12466; (*b*) A. Das, T. P. Mohammed and M. Sankaralingam, Biological Activity of Copper Porphyrins, *Coord. Chem. Rev.*, 2024, **506**, 215661.
6 A. Das and M. Sankaralingam, Are Zn(II) pincer complexes efficient apoptosis inducers? A deep insight into their activity against A549 lung cancer cells, *Dalton Trans.*, 2023, **52**, 14465–14476.
7 A. Das, R. Sangavi, S. Gowrishankar, R. Kumar and M. Sankaralingam, Deciphering the Mechanism of MRSA Targeting Copper(II) Complexes of NN_2 Pincer Type Ligands, *Inorg. Chem.*, 2023, **62**, 18926–18939.
8 (*a*) M. Sankaralingam, Y.-M. Lee, W. Nam and S. Fukuzumi, Amphoteric reactivity of metal–oxygen complexes in oxidation reactions, *Coord. Chem. Rev.*, 2018, **365**, 41–59; (*b*) M. Sankaralingam, Y.-M. Lee, D. G. Karmalkar, W. Nam and S. Fukuzumi, A mononuclear non-heme manganese (III)-aqua complex as a new active oxidant in hydrogen atom transfer reactions, *J. Am. Chem. Soc.*, 2018, **140**, 12695–12699; (*c*) M. Sankaralingam, Y.-M. Lee, Y. Pineda-Galvan, D. G. Karmalkar, M. S. Seo, S. H. Jeon, Y. Pushkar, S. Fukuzumi and W. Nam, Redox reactivity of a mononuclear manganese-oxo complex binding calcium ion and other redox-inactive metal ions, *J. Am. Chem. Soc.*, 2019, **141**, 1324–1336; (*d*) M. Sankaralingam, M. Balamurugan and M. Palaniandavar, Alkane and alkene oxidation reactions catalyzed by nickel(II) complexes: effect of ligand factors, *Coord. Chem. Rev.*, 2020, **403**, 213085; (*e*) W. P. Sohtun, S. Muthuramalingam, M. Sankaralingam, M. Velusamy and R. Mayilmurugan, Copper(II) Complexes of Tripodal Ligand Scaffold (N_3O) as Functional Models for Phenoxazinone Synthase, *J. Inorg. Biochem.*, 2021, **216**, 111313; (*f*) T. P. Mohammed and M. Sankaralingam, Reactivities of high valent manganese-oxo porphyrins in aqueous medium, *Tetrahedron*, 2022, **103**, 132483; (*g*) A. Rajeev, M. Balamurugan and M. Sankaralingam, Rational design of first-row transition metal complexes as the catalysts for oxidation of arenes: A homogeneous approach, *ACS Catal.*, 2022, **12**, 9953–9982; (*h*) A. Rajeev and M. Sankaralingam, Highlights of Oxygen Atom

Transfer Reactions Catalysed by Nickel Complexes, *Oxygen Atom Transfer Reactions*, 2023, vol. 1, pp. 62–90; (*i*) S. Patra, A. Das, S. Bhunia, A. Rajeev and M. Sankaralingam, Electrocatalytic production of hydrogen using nickel complexes with tridentate N3 ligands, *Catal. Today*, 2023, **423**, 113972; (*j*) Y. Wang, H. Huang, Q. Zhang and P. Zhang, Chirality in Metal-Based Anticancer Agents, *Dalton Trans.*, 2018, **47**, 4017–4026.

9 (*a*) M. Sankaralingam, M. Balamurugan, M. Palaniandavar, P. Vadivelu and C. H. Suresh, Nickel(II) Complexes of Pentadentate N5 Ligands as Catalysts for Alkane Hydroxylation by Using *m*-CPBA as Oxidant: A Combined Experimental and Computational Study, *Chem. – Eur. J.*, 2014, **20**, 11346–11361; (*b*) M. Sankaralingam, P. Vadivelu and M. Palaniandavar, Novel nickel(II) complexes of sterically modified linear N4 ligands: effect of ligand stereoelectronic factors and solvent of coordination on nickel(II) spin-state and catalytic alkane hydroxylation, *Dalton Trans.*, 2017, **46**, 7181–7193; (*c*) M. Sankaralingam, Y.-M. Lee, W. Nam and S. Fukuzumi, Selective Oxygenation of Cyclohexene by Dioxygen via an Iron(v)-Oxo Complex-Autocatalyzed Reaction, *Inorg. Chem.*, 2017, **56**, 5096–5104; (*d*) C. Saracini, D. D. Malik, M. Sankaralingam, Y.-M. Lee, W. Nam and S. Fukuzumi, Enhanced Electron-Transfer Reactivity of a Long-Lived Photoexcited State of a Cobalt–Oxygen Complex, *Inorg. Chem.*, 2018, **57**, 10945–10952; (*e*) S. Muthuramalingam, M. Sankaralingam, M. Velusamy and R. Mayilmurugan, Catalytic Conversion of Atmospheric CO_2 into Organic Carbonates by Nickel(II) Complexes of Diazepane-Based N_4 Ligands, *Inorg. Chem.*, 2019, **58**, 12975–12985; (*f*) X. Lu, Y.-M. Lee, M. Sankaralingam, S. Fukuzumi and W. Nam, Catalytic Four-Electron Reduction of Dioxygen by Ferrocene Derivatives with a Nonheme Iron(III) TAML Complex, *Inorg. Chem.*, 2020, **59**, 18010–18017.

10 (*a*) H. Lim, C. Oh, M.-S. Park, H.-B. Park, C. Ahn, W. K. Bae, K. H. Yoo and S. Hong, Hint from an Enzymatic Reaction: Superoxide Dismutase Models Efficiently Suppress Colorectal Cancer Cell Proliferation, *J. Am. Chem. Soc.*, 2023, **145**, 16058–16068; (*b*) Y. Lee, C. Oh, J. Kim, M.-S. Park, W. K. Bae, K. H. Yoo and S. Hong, Bioinspired Nonheme Iron Complex That Triggers Mitochondrial Apoptotic Signalling Pathway Specifically for Colorectal Cancer Cells, *Chem. Sci.*, 2022, **13**, 737–747.

11 (*a*) E. J. Ge, A. I. Bush, A. Casini, P. A. Cobine, J. R. Cross, G. M. DeNicola, Q. P. Dou, K. J. Franz, V. M. Gohil, S. Gupta, S. G. Kaler, S. Lutsenko, V. Mittal, M. J. Petris, R. Polishchuk, M. Ralle, M. L. Schilsky, N. K. Tonks, L. T. Vahdat, L. Van Aelst, D. Xi, P. Yuan, D. C. Brady and C. J. Chang, Connecting Copper and Cancer: From Transition Metal Signalling to Metalloplasia, *Nat. Rev. Cancer*, 2022, **22**, 102–113; (*b*) C. Rajarajeswari, R. Loganathan, M. Palaniandavar, E. Suresh, A. Riyasdeen and M. A. Akbarsha, Copper(II) Complexes with 2NO and 3N Donor Ligands: Synthesis, Structures and Chemical Nuclease and Anticancer Activities, *Dalton Trans.*, 2013, **42**, 8347–8363; (*c*) A. Sîrbu, O. Palamarciuc, M. V. Babak, J. M. Lim, K. Ohui, E. A. Enyedy, S. Shova, D. Darvasiová, P. Rapta, W. H. Ang and V. B. Arion, Copper(II) Thiosemicarbazone Complexes Induce Marked ROS Accumulation and Promote Nrf2-Mediated Antioxidant Response in Highly Resistant Breast Cancer Cells, *Dalton Trans.*, 2017, **46**, 3833–3847.

12 C. Santini, M. Pellei, V. Gandin, M. Porchia, F. Tisato and C. Marzano, Advances in Copper Complexes as Anticancer Agents, *Chem. Rev.*, 2013, **114**, 815–862.

13 X. Mingjin, Z. Qihua, L. Fangfang, Y. Junru, Z. Jihong, X. Jingyuan and S. Xueru, Schiff Bases Copper(II) Anticancer Complex and its Preparation Method and Application, *Chinese Patent*, 107759491B, 2017.

14 K. M. K. Al-Zaydi, A. I. D. Al-Sulami and M. T. J. Basha, Heterocyclic Diazenyl Pyridinone Copper(II) Complexes as Pharmacological Antitumor Agents, *US Patent*, US11104692B1, 2021.

15 O. Afzal, S. Kumar, M. R. Haider, M. R. Ali, R. Kumar, M. Jaggi and S. A. Bawa, Review on Anticancer Potential of Bioactive Heterocycle Quinoline, *Eur. J. Med. Chem.*, 2015, **97**, 871–910.

16 O. O. Ajani, K. T. Iyaye and O. T. Ademosun, Recent Advances in Chemistry and Therapeutic Potential of Functionalized Quinoline Motifs – a Review, *RSC Adv.*, 2022, **12**, 18594–18614.

17 N. T. A. Dawoud, E. M. El-Fakharany, A. E. Abdallah, H. El-Gendi and D. R. Lotfy, Synthesis, and Docking Studies of Novel Heterocycles Incorporating the Indazolylthiazole Moiety as Antimicrobial and Anticancer Agents, *Sci. Rep.*, 2022, **12**, 3424.

18 V. R. Solomon, S. Pundir and H. Lee, Examination of Novel 4-Aminoquinoline Derivatives Designed and Synthesized by a Hybrid Pharmacophore Approach to Enhance Their Anticancer Activities, *Sci. Rep.*, 2019, **9**, 6315.

19 B. Kundu, S. K. Das, S. P. Chowdhuri, S. Pal, D. Sarkar, A. Ghosh, A. Mukherjee, D. Bhattacharya, B. B. Das and A. Talukdar, Discovery and Mechanistic Study of Tailor-Made Quinoline Derivatives as Topoisomerase 1 Poison with Potent Anticancer Activity, *J. Med. Chem.*, 2019, **62**, 3428–3446.

20 G. Gasser, I. Ott and N. Metzler-Nolte, Organometallic Anticancer Compounds, *J. Med. Chem.*, 2011, **54**, 3–25.

21 A. P. Kourounakis, D. Xanthopoulos and A. Tzara, Morpholine as a Privileged Structure: A Review on the Medicinal Chemistry and Pharmacological Activity of Morpholine Containing Bioactive Molecules, *Med. Res. Rev.*, 2020, **40**, 709–752.

22 (*a*) N. Takahashi, T. Honda and T. Ohba, Anticancer and Superoxide Scavenging Activities of P-Alkylaminophenols Having Various Length Alkyl Chains, *Bioorg. Med. Chem.*, 2006, **14**, 409–417; (*b*) F. Hackenberg and M. Tacke, Benzyl-Substituted Metallocarbene Antibiotics and Anticancer Drugs, *Dalton Trans.*, 2014, **43**, 8144–8153.

23 S. Wu, Z. Wu, Q. Ge, X. Zheng and Z. Yang, Antitumor Activity of Tridentate Pincer and Related Metal Complexes, *Org. Biomol. Chem.*, 2021, **19**, 5254.

24 S. Zhang, C. Tu, X. Wang, Z. Yang, J. Zhang, L. Lin, J. Ding and Z. Guo, Novel Cytotoxic Copper(II) Complexes of 8-Aminoquinoline Derivatives: Crystal Structure and Different Reactivity towards Glutathione, *Eur. J. Inorg. Chem.*, 2004, **2004**, 4028–4035.

25 J. Lu, Q. Sun, J.-L. Li, L. Jiang, W. Gu, X. Liu, J.-L. Tian and S.-P. Yan, Two Water-Soluble Copper(II) Complexes: Synthesis, Characterization, DNA Cleavage, Protein Binding Activities and in Vitro Anticancer Activity Studies, *J. Inorg. Biochem.*, 2014, **137**, 46–56.

26 K. Czerwińska, B. Machura, S. Kula, S. Krompiec, K. Erfurt, C. Roma-Rodrigues, A. R. Fernandes, L. S. Shul'pina, N. S. Ikonnikov and G. B. Shul'pin, Copper(II) Complexes of Functionalized 2,2′:6′,2″-terpyridines and 2,6-di(Thiazol-2-yl)pyridine: Structure, Spectroscopy, Cytotoxicity and Catalytic Activity, *Dalton Trans.*, 2017, **46**, 9591–9604.

27 L. Tabrizi and H. Chiniforoshan, Synthesis and C–H Activation Reactions of Cyclometalated Copper(I) Complexes with NCN Pincer and 1,3,5-Triaza-7-Phosphaadamantane Derivatives: In Vitro Antimicrobial and Cytotoxic Activity, *New J. Chem.*, 2017, **41**, 10972–10984.

28 H. G. Sogukomerogullari and S. Akkoc, Copper(II) Complexes with Thioether based SNS Pincer Ligand: Synthesis, Characterization and Antiproliferative Activity, *J. Struct. Chem.*, 2023, **64**, 157–167.

29 A. Das and M. Sankaralingam, Method for preparing a potent copper(II) complex as an apoptosis inducer in lung cancer, *Indian Patent*, 518352, 2024.

30 SADABS, *Ver. 2.05, SMART, Ver. 5.631, and SAINT, v 6.45*, Bruker AXS Inc., Madison, WI, 2003.

31 G. M. Sheldrick, Crystal structure refinement with SHELXL, *Acta Crystallogr., Sect. C: Struct. Chem.*, 2015, **71**, 3–8.

32 L. J. Farrugia, WinGX and ORTEP for Windows: an update, *J. Appl. Crystallogr.*, 2012, **45**, 849–854.

33 M. Alley, D. A. Scudiero, A. Monks, M. L. Hursey, M. Czerwinski, D. L. Fine, B. J. Abbott, J. A. Mayo, R. H. Shoemaker and M. R. Boyd, Feasibility of Drug Screening with Panels of Human Tumor Cell Lines Using a Microculture Tetrazolium Assay, *Cancer Res.*, 1988, **48**, 589–601.

34 Z. Mao, Z. Liu, L. Chen, J. Yang, B. Zhao, Y. M. Jung, X. Wang and C. Zhao, Predictive Value of the Surface-Enhanced Resonance Raman Scattering-Based MTT Assay: A Rapid and Ultrasensitive Method for Cell Viability in Situ, *Anal. Chem.*, 2013, **85**, 7361–7368.

35 G. M. Asong, F. Amissah, C. Voshavar, A. T. Nkembo, E. Ntantie, N. S. Lamango and S. Y. Ablordeppey, A Mechanistic Investigation on the Anticancer Properties of SYA013, a Homopiperazine Analogue of Haloperidol with Activity against Triple Negative Breast Cancer Cells, *ACS Omega*, 2020, **5**, 32907–32918.

36 D. Ribble, N. B. Goldstein, D. A. Norris and Y. G. Shellman, A simple technique for quantifying apoptosis in 96-well plates, *BMC Biotechnol.*, 2005, **5**, 32907–32918.

37 K. Liu, P.-C. Liu, R. Liu and X. Wu, Dual AO/EB Staining to Detect Apoptosis in Osteosarcoma Cells Compared with Flow Cytometry, *Med. Sci. Monit. Basic Res.*, 2015, **21**, 15–20.

38 I. Vermes, C. Haanen and C. Reutelingsperger, Flow Cytometry of Apoptotic Cell Death, *J. Immunol. Methods*, 2000, **243**, 167–190.

39 V. V. Shynkar, A. S. Klymchenko, C. Kunzelmann, G. Duportail, C. D. Muller, A. P. Demchenko, J.-M. Freyssinet and Y. Mely, Fluorescent Biomembrane Probe for Ratiometric Detection of Apoptosis, *J. Am. Chem. Soc.*, 2007, **129**, 2187–2193.

40 D. Wlodkowic, J. Skommer and Z. Darzynkiewicz, Flow Cytometry-Based Apoptosis Detection, *Methods Mol. Biol.*, 2009, **559**, 19–32.

41 Y. Qiu, E. Rojas, R. A. Murray, J. Irigoyen, D. Gregurec, P. Castro-Hartmann, J. Fledderman, I. Estrela-Lopis, E. Donath and S. E. Moya, Cell Uptake, Intracellular Distribution, Fate and Reactive Oxygen Species Generation of Polymer Brush Engineered CeO_{2-X}NPs, *Nanoscale*, 2015, **7**, 6588–6598.

42 C. Xu, R. Song, P. Lu, J. Chen, Y. Zhou, G. Shen, M. Jiang and W. Zhang, A pH-Responsive Charge-Reversal Drug Delivery System with Tumor-Specific Drug Release and ROS Generation for Cancer Therapy, *Int. J. Nanomedicine.*, 2020, **15**, 65–80.

43 H. Zhao, J. Huang, Y. Li, X. Lv, H. Zhou, H. Wang, Y. Xu, C. Wang, J. Wang and Z. Liu, ROS-Scavenging Hydrogel to Promote Healing of Bacteria Infected Diabetic Wounds, *Biomaterials*, 2020, **258**, 120286.

44 (*a*) M. Reers, S. T. Smiley, C. Mottola-Hartshorn, A. Chen, M. Lin and L. B. Chen, Mitochondrial Membrane Potential Monitored by JC-1 Dye, *Methods Enzymol.*, 1995, **260**, 406–417.

45 P. C. Saha, T. Chatterjee, R. Pattanayak, R. S. Das, A. Mukherjee, M. Bhattacharyya and S. Guha, Targeting and Imaging of Mitochondria Using Near-Infrared Cyanine Dye and Its Application to Multicolor Imaging, *ACS Omega*, 2019, **4**, 14579–14588.

46 F. Sivandzade, A. Bhalerao and L. Cucullo, Analysis of the Mitochondrial Membrane Potential Using the Cationic JC-1 Dye as a Sensitive Fluorescent Probe, *Bio-Protoc.*, 2019, **9**, e3128.

47 M. F. Harris and J. L. Logan, Determination of Log K_{ow} Values for Four Drugs, *J. Chem. Educ.*, 2014, **91**, 915–918.

48 O. Trott and A. J. Olson, *J. Comput. Chem.*, 2010, **31**, 455–461.

49 M. J. Frisch, G. W. Trucks, H. B. Schlegel, G. E. Scuseria, M. A. Robb, J. R. Cheeseman, G. Scalmani, V. Barone, B. Mennucci, G. A. Petersson, H. Nakatsuji, M. Caricato, X. Li, H. P. Hratchian, A. F. Izmaylov, J. Bloino, G. Zheng, J. L. Sonnenberg, M. Hada, M. Ehara, K. Toyota, R. Fukuda, J. Hasegawa, M. Ishida, T. Nakajima, Y. Honda, O. Kitao, H. Nakai, T. Vreven, J. A. Montgomery Jr., J. E. Peralta, F. Ogliaro, M. Bearpark, J. J. Heyd, E. Brothers, K. N. Kudin, V. N. Staroverov, R. Kobayashi, J. Normand, K. Raghavachari, A. Rendell, J. C. Burant, S. S. Iyengar, J. Tomasi, M. Cossi, N. Rega, J. M. Millam, M. Klene,

J. E. Knox, J. B. Cross, V. Bakken, C. Adamo, J. Jaramillo, R. Gomperts, R. E. Stratmann, O. Yazyev, A. J. Austin, R. Cammi, C. Pomelli, J. W. Ochterski, R. L. Martin, K. Morokuma, V. G. Zakrzewski, G. A. Voth, P. Salvador, J. J. Dannenberg, S. Dapprich, A. D. Daniels, O. Farkas, J. B. Foresman, J. V. Ortiz, J. Cioslowski and D. J. Fox, *Gaussian 09 Revision A.02*, Gaussian Inc., Wallingford CT, 2009.

50 Accelrys Software Inc, *Discovery Studio Modeling Environment, Release 4.0*, Accelrys Software Inc., San Diego, 2013.

51 (*a*) A. S. Thennarasu, T. P. Mohammed and M. Sankaralingam, Mononuclear Copper(II) Schiff Base Complexes as Effective Models for Phenoxazinone Synthase, *New J. Chem.*, 2022, **46**, 21684–21694; (*b*) T. P. Mohammed, A. George, M. P. Sivaramakrishnan, P. Vadivelu, S. Balasubramanian and M. Sankaralingam, Deciphering the Effect of Amine versus Imine Ligands of Copper(II) Complexes in 2-Aminophenol Oxidation, *J. Inorg. Biochem.*, 2023, **247**, 112309.

52 (*a*) B. J. Hathaway and D. E. Billing, The Electronic Properties and Stereochemistry of Mono-Nuclear Complexes of the Copper(II) Ion, *Coord. Chem. Rev.*, 1970, **5**, 143–207; (*b*) E. Garribba and G. Micera, The Determination of the Geometry of Cu(II) Complexes: An EPR Spectroscopy Experiment, *J. Chem. Educ.*, 2006, **83**, 1229.

53 (*a*) E. Billig, R. Williams, I. Bernal, J. H. Waters and H. B. Gray, The Electronic Structures of Square-Planar Metal Complexes. II. The Complexes of Maleonitriledithiolate with Copper(II), Nickel(II), Palladium (II), and Platinum(II), *Inorg. Chem.*, 1964, **3**, 663–666; (*b*) M. M. Bhadbhade and D. Srinivas, Effects on Molecular Association, Chelate Conformation, and Reactivity toward Substitution in Copper Cu(5-X-Salen) Complexes, Salen^{2-} = *N,N′*-Ethylenebis(Salicylidenaminato), X = H, CH_3O, and Cl: Synthesis, X-Ray Structures, and EPR Investigations, *Inorg. Chem.*, 1993, **32**, 5458–5466; (*c*) G. Verquin, G. Fontaine, E. Abi-Aad, E. Zhilinskaya, A. Aboukaïs and J.-L. Bernier, EPR Study of Copper(II) Complexes of Hydroxysalen Derivatives in Order to be Used in the DNA Cleavage, *J. Photochem. Photobiol., B.*, 2007, **86**, 272–278.

54 A. G. Blackman, E. B. Schenk, R. E. Jelley, E. H. Krenske and L. R. Gahan, Five-Coordinate Transition Metal Complexes and the Value of τ_5: Observations and Caveats, *Dalton Trans.*, 2020, **49**, 14798–14806.

55 G. Abbas, G. Pandey, K. B. Singh and N. Gautam, One-Pot Surface Modification of β-Cu_2O NPs for Biocatalytic Performance against A-549 Lung Carcinoma Cell Lines through Docking Analysis, *ACS Omega*, 2021, **6**, 29380–29393.

56 S. E. Salamifar and R. Y. Lai, Use of Combined Scanning Electrochemical and Fluorescence Microscopy for Detection of Reactive Oxygen Species in Prostate Cancer Cells, *Anal. Chem.*, 2013, **85**, 9417–9421.

57 M. d. P. S. Idelchik, U. Begley, T. J. Begley and J. A. Melendez, Mitochondrial ROS Control of Cancer, *Semin. Cancer Biol.*, 2017, **47**, 57–66.

58 E. Gottlieb, S. M. Armour, M. H. Harris and C. B. Thompson, Mitochondrial Membrane Potential Regulates Matrix Configuration and Cytochrome *c* Release during Apoptosis, *Cell Death Differ.*, 2003, **10**, 709–717.

59 S. N. Krishnan, J. L. Rosales and K.-Y. Lee, ROS-Mediated Cancer Cell Killing through Dietary Phytochemicals, *Oxid. Med. Cell. Longevity*, 2019, **2019**, 1–16.

60 S. S. Sabharwal and P. T. Schumacker, Mitochondrial ROS in Cancer: Initiators, Amplifiers or an Achilles' Heel?, *Nat. Rev. Cancer*, 2014, **14**, 709–721.

61 S. Mohapatra, G. Das, V. Gupta, P. Mondal, M. Nitani, Y. Ie, S. Chatterjee, Y. Aso and S. Ghosh, Power of an Organic Electron Acceptor in Modulation of Intracellular Mitochondrial Reactive Oxygen Species: Inducing JNK- and Caspase-Dependent Apoptosis of Cancer Cells, *ACS Omega*, 2021, **6**, 7815–7828.

62 B. Perillo, M. Di Donato, A. Pezone, E. Di Zazzo, P. Giovannelli, G. Galasso, G. Castoria and A. Migliaccio, ROS in Cancer Therapy: The Bright Side of the Moon, *Exp. Mol. Med.*, 2020, **52**, 192–203.

63 R. G. Efremov, R. Baradaran and L. A. Sazanov, The Architecture of Respiratory Complex I, *Nature*, 2010, **465**, 441–445.

64 R. Guo, S. Zong, M. Wu, J. Gu and M. Yang, Architecture of Human Mitochondrial Respiratory Megacomplex $I_2III_2IV_2$, *Cell*, 2017, **170**, 1247–1257.

65 P. Saura and V. R. I. Kaila, Energetics and Dynamics of Proton-Coupled Electron Transfer in the NADH/FMN Site of Respiratory Complex I, *J. Am. Chem. Soc.*, 2019, **141**, 5710–5719.